
Improving the Gating Mechanism of Recurrent Neural Networks

Albert Gu¹ Caglar Gulcehre² Tom Paine² Matt Hoffman² Razvan Pascanu²

Abstract

Gating mechanisms are widely used in neural network models, where they allow gradients to backpropagate more easily through depth or time. However, their saturation property introduces problems of its own. For example, in recurrent models these gates need to have outputs near 1 to propagate information over long time-delays, which requires them to operate in their saturation regime and hinders gradient-based learning of the gate mechanism. We address this problem by deriving two synergistic modifications to the standard gating mechanism that are easy to implement, introduce no additional hyperparameters, and improve learnability of the gates when they are close to saturation. We show how these changes are related to and improve on alternative recently proposed gating mechanisms such as chrono initialization and Ordered Neurons. Empirically, our simple gating mechanisms robustly improve the performance of recurrent models on a range of applications, including synthetic memorization tasks, sequential image classification, language modeling, and reinforcement learning, particularly when long-term dependencies are involved.

1. Introduction

Recurrent neural networks (RNNs) are an established machine learning tool for learning from sequential data. However, RNNs are prone to the vanishing gradient problem, which occurs when the gradients of the recurrent weights become vanishingly small as they get backpropagated through time (Hochreiter, 1991; Bengio et al., 1994; Hochreiter et al., 2001). A common approach to alleviate the vanishing gradient problem is to use gating mechanisms, leading to models such as the long short term memory (Hochreiter & Schmidhuber, 1997, LSTM) and gated recurrent units

(Chung et al., 2014, GRUs). These gated RNNs have been very successful in several different application areas such as in reinforcement learning (Kapturowski et al., 2018; Espeholt et al., 2018) and natural language processing (Bahdanau et al., 2014; Kočiský et al., 2018).

At every time step, gated recurrent networks use a weighted combination of the history summarized by the previous state, and a function of the incoming inputs, to create the next state. The values of the gates, which are the coefficients of the weighted combination, control the length of temporal dependencies that can be addressed. This weighted update can be seen as an additive or residual connection on the recurrent state, which helps signals propagate through time without vanishing. However, the gates themselves are prone to a saturating property which can also hamper gradient-based learning. This can be problematic for RNNs, where carrying information for very long time delays requires gates to be very close to their saturated states.

We address two particular problems that arise with the standard gating mechanism of recurrent models. Firstly, learning when gates are in their saturation regime is difficult because gradients through the gates vanish as they saturate. We derive a modification to standard gating mechanisms that uses an auxiliary *refine gate* (Section 3.1) to modulate a main gate. This mechanism allows the gates to have a wider range of activations without gradients vanishing as quickly. Secondly, typical initialization of the gates is relatively concentrated. This restricts the range of timescales the model can address at initialization, as the timescale of a particular unit is dictated by its gates. We propose *uniform gate initialization* (Section 3.2) that addresses this problem by directly initializing the activations of these gates from a distribution that captures a wider spread of dependency lengths.

The main contribution of this paper is the **refine** gate mechanism. As the refine gate works better in tandem with uniform gate initialization, we call this combination the **UR** gating mechanism. We focus on comparing the UR gating mechanism against other approaches in our experiments. These changes can be applied to any gate (i.e. parameterized bounded function) and have minimal to no overhead in terms of speed, memory, code complexity, parameters, or hyperparameters. We apply them to the forget gate of recurrent models, and evaluate on several benchmark tasks that re-

¹Stanford University, USA ²DeepMind, London, UK. Correspondence to: Albert Gu <albertgu@stanford.edu>, Caglar Gulcehre <caglarg@google.com>.

quire long-term memory including synthetic memory tasks, pixel-by-pixel image classification, language modeling, and reinforcement learning. Finally, we connect our methods to other proposed gating modifications, introduce a framework that allows each component to be replaced with similar ones, and perform extensive ablations of our method. Empirically, the UR gating mechanism robustly improves on the standard forget and input gates of gated recurrent models. When applied to the LSTM, these simple modifications solve synthetic memory tasks that are pathologically difficult for the standard LSTM, achieve state-of-the-art results on sequential MNIST and CIFAR-10, and show consistent improvements in language modeling on the WikiText-103 dataset (Merity et al., 2016) and reinforcement learning tasks (Hung et al., 2018).

2. Gated Recurrent Neural Networks

Broadly speaking, RNNs are used to sweep over a sequence of input data x_t to produce a sequence of recurrent states $h_t \in \mathbb{R}^d$ summarizing information seen so far. At a high level, an RNN is just a parametrized function in which each sequential application of the network computes a state update $u: (x_t, h_{t-1}) \mapsto h_t$. Gating mechanisms were introduced to address the vanishing gradient problem (Hochreiter, 1991; Bengio et al., 1994; Hochreiter et al., 2001), and have proven to be crucial to the success of RNNs. This mechanism essentially smooths out the update using the following equation,

$$h_t = f_t(x_t, h_{t-1}) \circ h_{t-1} + i_t(x_t, h_{t-1}) \circ u(x_t, h_{t-1}), \quad (1)$$

where the *forget gate* f_t and *input gate* i_t are $[0, 1]^d$ -valued functions that control how fast information is forgotten or allowed into the memory state. When the gates are tied, i.e. $f_t + i_t = 1$ as in GRUs, they behave as a low-pass filter, deciding the time-scale on which the unit will respond (Tallec & Ollivier, 2018). For example, large forget gate activations close to $f_t = 1$ are necessary for recurrent models to address long-term dependencies.¹

We will introduce our improvements to the gating mechanism primarily in the context of the LSTM, which is the most popular recurrent model.

$$f_t = \sigma(\mathcal{P}_f(x_t, h_{t-1})), \quad (2)$$

$$i_t = \sigma(\mathcal{P}_i(x_t, h_{t-1})), \quad (3)$$

$$u_t = \tanh(\mathcal{P}_u(x_t, h_{t-1})), \quad (4)$$

$$c_t = f_t \circ c_{t-1} + i_t \circ u_t, \quad (5)$$

$$o_t = \sigma(\mathcal{P}_o(x_t, h_{t-1})), \quad (6)$$

$$h_t = o_t \tanh(c_t). \quad (7)$$

A typical LSTM (equations (2)-(7)) is an RNN whose state is represented by a tuple (h_t, c_t) consisting of a “hidden”

¹In this work, we use “gate” to alternatively refer to a $[0, 1]$ -valued function or the value (“activation”) of that function.

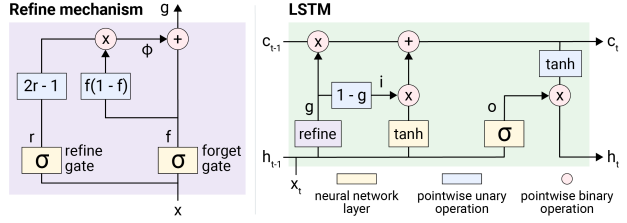


Figure 1. Refine mechanism. The refine mechanism improves flow of gradients through a saturating gate f . As f saturates, its gradient vanishes, and its value is unlikely to change (see Figure 4). The refine gate r is used to produce a bounded additive term ϕ that may push f lower or higher as necessary. The resulting effective gate g can achieve values closer to 0 and 1 and can change even when f is stuck. We apply it to the forget gate of an LSTM. The g is then used in place of f in the state update (5).

state and “cell” state. The state update equation (1) is used to create the next cell state c_t (5). Note that the gate and update activations are a function of the previous hidden state h_{t-1} instead of c_{t-1} . Here, \mathcal{P}_* stands for a parameterized linear function of its inputs with bias b_* , e.g.

$$\mathcal{P}_f(x_t, h_{t-1}) = W_{fx}x_t + W_{fh}h_{t-1} + b_f. \quad (8)$$

and $\sigma(\cdot)$ refers to the standard sigmoid activation function which we will assume is used for defining $[0, 1]$ -valued activations in the rest of this paper. The gates of the LSTM were initially motivated as a binary mechanism, switching on or off, allowing information and gradients to pass through. However, in reality, this fails to happen due to a combination of two factors: initialization and saturation. This can be problematic, such as when very long dependencies are present.

3. Our Proposed Gating Mechanisms

We present two solutions that work in tandem to address the previously described issues. The first is the **refine gate**, which allows for better gradient flow by reparameterizing a saturating gate, for example, the forget gate. The second is **uniform gate initialization**, which ensures a diverse range of gate values are captured at the start of training, which allows a recurrent model to have a multi-scale representation of an input sequence at initialization.

3.1. Refine Gate

Formally, the full mechanism of the refine gate as applied to gated recurrent models is defined in equations (9)-(11). Note that it is an isolated change where the forget gate f_t is modified to get the effective forget gate in (10) before applying the the standard update (1). Figure 1 illustrates the refine gate in an LSTM cell. Figure 3 illustrates how the refine gate r_t is defined and how it changes the forget gate f_t to produce an effective gate g_t . The refine gate allows the effective gate g to reach much higher and lower activations than the

constituent gates f and r , bypassing the saturating gradient problem. For example, this allows the effective forget gate to reach $g = 0.99$ when the forget gate is only $f = 0.9$.

Finally, to simplify comparisons and ensure that we always use the same number of parameters as the standard gates, when using the refine gate we tie the input gate to the effective forget gate, $i_t = 1 - g_t$.² However, we emphasize that these techniques can be applied to any gate (or more broadly, any bounded function) to improve initialization distribution and help optimization. For example, our methods can be combined in different ways in recurrent models, e.g. an independent input gate can be modified with its own refine gate.

$$r_t = \sigma(\mathcal{P}_r(x_t, h_{t-1})), \quad (9)$$

$$g_t = r_t \cdot (1 - (1 - f_t)^2) + (1 - r_t) \cdot f_t^2, \quad (10)$$

$$c_t = g_t c_{t-1} + (1 - g_t) u_t. \quad (11)$$

3.2. Uniform Gate Initialization

Standard initialization schemes for the gates can prevent the learning of long-term temporal correlations (Tallec & Ollivier, 2018). For example, supposing that a unit in the cell state has constant forget gate value f_t , then the contribution of an input x_t in k time steps will decay by $(f_t)^k$. This gives the unit an effective *decay period* or *characteristic timescale* of $O(\frac{1}{1-f_t})$.³ Standard initialization of linear layers \mathcal{L} sets the bias term to 0, which causes the forget gate values (2) to concentrate around 0.5. A common trick of setting the forget gate bias to $b_f = 1.0$ (Jozefowicz et al., 2015) does increase the value of the decay period to $\frac{1}{1-\sigma(1.0)} \approx 3.7$. However, this is still relatively small and may hinder the model from learning dependencies at varying timescales easily.

We instead propose to directly control the distribution of forget gates, and hence the corresponding distribution of decay periods. In particular, we propose to simply initialize the value of the forget gate activations f_t according to a uniform distribution $\mathcal{U}(0,1)$ ⁴,

$$b_f \sim \sigma^{-1}(\mathcal{U}[\epsilon, 1-\epsilon]). \quad (12)$$

An important difference between UGI and standard or other (e.g. Tallec & Ollivier, 2018) initializations is that negative forget biases are allowed. The effect of UGI is that all timescales are covered, from units with very high forget activations remembering information (nearly) indefinitely, to those with low activations focusing solely on the incoming

²In our experiments, we found that tying input/forget gates makes negligible difference on downstream performance, consistent with previous findings in the literature (Greff et al., 2016; Melis et al., 2017).

³This corresponds to the number of timesteps it takes to decay by $1/e$.

⁴Since $\sigma^{-1}(0) = -\text{inf}$, we use the standard practice of thresholding with a small ϵ for stability.

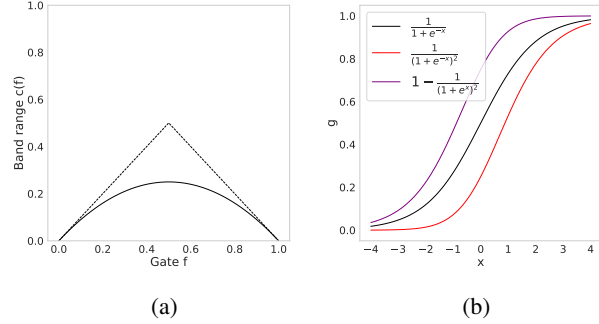


Figure 2. **The adjustment function.** (a) An adjustment function $\alpha(f_t)$ satisfying natural properties is chosen to define a band within which the forget gate is refined. (b) The forget gate $f_t(x)$ is conventionally defined with the sigmoid function (black). The refine gate interpolates around the original gate f_t to yield an effective gate g_t within the upper and lower curves, $g_t \in f_t \pm \alpha(f_t)$.

input. Additionally, it introduces no additional parameters; it even can have less hyperparameters than the standard gate initialization, which sometimes tunes the forget bias b_f (Jozefowicz et al., 2015). Appendix B.2 and B.3 further discuss the theoretical effects of UGI on timescales.

3.3. The URLSTM

The URLSTM requires two small modifications to the vanilla LSTM. First, we present the way the biases of forget gates are initialized in Equation (12) with UGI. Second, the modifications on the standard LSTM equations to compute the refine and effective forget gates are presented in Equations (9)-(11). However, we note that these methods can be used to modify any gate (or more generally, bounded function) in any model. In this context, the URLSTM is simply defined by applying UGI and a refine gate r on the original forget gate f to create an effective forget gate g (Equation (10)). This effective gate is then used in the cell state update (11). Empirically, these small modifications to an LSTM are enough to allow it to achieve nearly binary activations and solve difficult memory problems (Figure 5).

3.4. A Formal Treatment of Refine Gates

Given a gate $f = \sigma(\mathcal{P}_f(x)) \in [0, 1]$, the refine gate is an independent gate $r = \sigma(\mathcal{P}_r(x))$ that modulates f to produce a value $g \in [0, 1]$ which will be used in place of f downstream. It is motivated by considering how to modify the output of a gate f in a way that promotes gradient-based learning, derived below.

An additive adjustment A root cause of the saturation problem is that the gradient ∇f of a gate can be written solely as a function of the activation value as $f(1-f)$, decays rapidly as f approaches to 0 or 1. Thus when the activation f is past a certain upper or lower threshold,

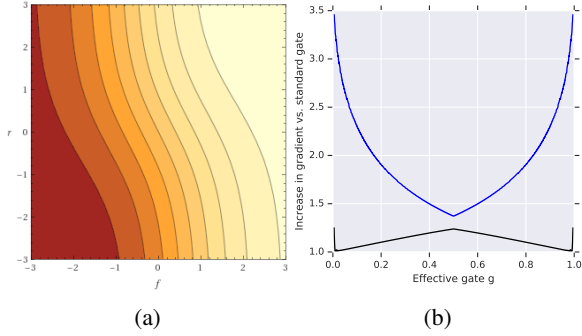


Figure 3. Refine gate activations and gradients.: (a) Contours of the effective gate g_t as a function of the forget and refine gates f_t, r_t . High effective activations can be achieved with more modest f_t, r_t values. (b) The gradient ∇g_t as a function of effective gate activation g_t . [Black, blue]: Lower and upper bounds on the ratio of the gradient with a refine gate vs. the gradient of a standard gate. For activation values near the extremes, the refine gate can significantly increase the gradients.

learning effectively stops. This problem cannot be fully addressed only by modifying the input of the sigmoid, as in UGI and other techniques, as the gradient will still vanish by backpropagating through the activation function.

Therefore to better control activations near the saturating regime, instead of changing the input to the sigmoid in $f = \sigma(\mathcal{P}(x))$, we consider modifying the output. Modifying the gate with a multiplicative interaction can have unstable learning dynamics since when the gates have very small values, the multiplicative factor may need to be very large to avoid the gradients of the gates shrinking to zero. As a result, we consider adjusting f with an input-dependent additive update $\phi(f, x)$ for some function ϕ , to create an effective gate $g = f + \phi(f, x)$ that will be used in place of f downstream such as in the main state update (1). This sort of additive (“residual”) connection is a common technique to increase gradient flow, and indeed was the motivation of the LSTM additive gated update (1) itself (Hochreiter & Schmidhuber, 1997).

Choosing the adjustment function ϕ Although there might be many choices that seem plausible for choosing an appropriate additive update ϕ , we first identify the desirable properties of such a function and then discuss how our refine gate mechanism satisfies those properties.

The desired properties of ϕ emerge considering the applications of the gating mechanisms in recurrent models:

- **Boundedness:** After the additive updates, the activations still need to be bounded between 0 and 1.
- **Symmetry:** The resulting gating framework should be symmetric around 0, as sigmoid does.
- **Smoothness:** The refining mechanism should be differentiable, since we will be using backpropagation

and gradient based optimization methods.

Let us note that, f_t may need to be either increased or decreased, regardless of what value it has. This is because the gradients through the gates can vanish either when the activations get closer to 0 or 1. Therefore, an additive update to f should create an *effective gate activation* g_t in the range $f_t \pm \alpha$ for some α . We assume that the allowed adjustment range, $\alpha = \alpha(f_t)$, needs to be a function of f to keep the g between 0 and 1. Since 0 and 1 are symmetrical in the gating framework, our adjustment rate should also satisfy $\alpha(f) = \alpha(1 - f)$.

Figure 2a illustrates the general appearance of $\alpha(f)$ based on aforementioned properties. According to the *Boundedness* property, the adjustment rate should be upper-bounded by $\min(f, 1 - f)$ to ensure that $g \in f \pm \alpha(f)$ is bounded between 0 and 1. As a consequence of this property, its derivatives should also satisfy, $\alpha'(0) \leq 1$ and $\alpha'(1) \geq -1$. Symmetry also implies $\alpha'(f) = -\alpha'(1 - f)$, and smoothness implies α' is continuous. The simplest such function satisfying all these properties is the linear $\alpha'(f) = 1 - 2f$, yielding to our choice of adjustment function, $\alpha(f) = f - f^2 = f(1 - f)$. However, when f is bounded between 0 and 1, $\alpha(f)$ will be positive.

Recall that the goal is to produce an effective activation $g = f + \phi(f, x)$ such that $g \in f \pm \alpha(f)$ (Figure 2b) given. Our final observation is that the simplest such function ϕ satisfying this is $\phi(f, x) = \alpha(f)\psi(f, x)$ where $\psi(f, x) \in [-1, 1]$ decides the sign of adjustment, and it can also change its magnitude as well. The standard method of defining $[-1, 1]$ -valued differentiable functions is achieved by using a tanh non-linearity, and this leads to $\phi(f, x) = \alpha(f)(2r - 1)$ for another gate $r = \sigma(\mathcal{P}(x))$. The full refine update equation can be given as in Equation (13),

$$\begin{aligned} g &= f + \alpha(f)(2r - 1) = f + f(1 - f)(2r - 1) \\ &= (1 - r) \cdot f^2 + r \cdot (1 - (1 - f)^2) \end{aligned} \quad (13)$$

Equation (13) has the elegant interpretation that the gate r linearly interpolates between the lower band $f - \alpha(f) = f^2$ and the symmetric upper band $f + \alpha(f) = 1 - (1 - f)^2$ (Figure 2b). In other words, the original gate f is the coarse-grained determinant of the effective gate g , while the gate r “refines” it.

4. Related Gating Mechanisms

We highlight a few recent works that also propose small gate changes to address problems of long-term or variable-length dependencies. Like ours, they can be applied to any gated update equation.

Tallic & Ollivier (2018) suggest an initialization strategy to capture long-term dependencies on the order of T_{max} , by sampling the gate biases from $b_f \sim \log \mathcal{U}(1, T_{max} - 1)$. Although similar to UGI in definition, *chrono initialization*

(CI) has critical differences in the timescales captured, for example, by using an explicit timescale parameter and having no negative biases. Due to its relation to UGI, we provide a more detailed comparison in Appendix B.3. As mentioned in Section 3.4, techniques such as these that only modify the input to a sigmoid gate do not adequately address the saturation problem.

The Ordered Neuron (ON) LSTM introduced by (Shen et al., 2018) aims to induce an ordering over the units in the hidden states such that “higher-level” neurons retain information for longer and capture higher-level information. We highlight this work due to its recent success in NLP, and also because its novelties can be factored into introducing two mechanisms which only affect the forget and input gates, namely (i) the $\text{cumax} := \text{cumsum} \circ \text{softmax}$ activation function which creates a monotonically increasing vector in $[0,1]$, and (ii) a pair of “master gates” which are ordered by cumax and fine-tuned with another pair of gates.

We observe that these are related to our techniques in that one controls the distribution of a gate activation, and the other is an auxiliary gate with modulating behavior. Despite its important novelties, we find that the ON-LSTM has drawbacks, including speed and scaling issues of its gates. We provide the formal definition and detailed analysis of the ON-LSTM in Appendix B.4. For example, we comment on how UGI can also be motivated as a faster approximation of the cumax activation. We also flesh out a deeper relationship between the master and refine gates and show how they can be interchanged for each other.

We include a more thorough overview of other related works on RNNs in Appendix B.1. These methods are mostly orthogonal to the isolated gate changes considered here and are not analyzed. We note that an important drawback common to all other approaches is the introduction of substantial hyperparameters in the form of constants, training protocol, and significant architectural changes. For example, even for chrono initialization, one of the less intrusive proposals, we experimentally find it to be particularly sensitive to the hyperparameter T_{max} (Section 5).

4.1. Gate Ablations

Our insights about previous work with related gate components allow us to perform extensive ablations of our contributions. We observe two independent axes of variation, namely, activation function/initialization (cumax , constant bias sigmoid, CI, UGI) and auxiliary modulating gates (master, refine), where different components can be replaced with each other. Therefore we propose several other gate combinations to isolate the effects of different gating mechanisms. We summarize a few ablations here; precise details are given in Appendix B.5. **O-**: Ordered gates. A natural simplification of the main idea of ON-LSTM, while keeping the hierarchical

Table 1. **Summary of gate ablations.** Summary of gating mechanisms considered in this work as applied to the forget/input gates of recurrent models. Some of these ablations correspond to previous work. -- standard LSTMs, C- (Tallec & Ollivier, 2018), and OM (Shen et al., 2018)

Name	Initialization/Activation	Auxiliary Gate
--	Standard initialization	N/A
C-	Chrono initialization	N/A
O-	cumax activation	N/A
U-	Uniform initialization	N/A
-R	Standard initialization	Refine gate
OM	cumax activation	Master gate
UM	Uniform initialization	Master gate
OR	cumax activation	Refine gate
UR	Uniform initialization	Refine gate

bias on the forget activations, is to simply drop the auxiliary master gates and define f_t, i_t (2)-(3) using the cumax activation function. **UM**: UGI master gates. This variant of the ON-LSTM’s gates ablates the cumax operation on the master gates, replacing it with a sigmoid activation and UGI which maintains the same initial distribution on the activation values. **OR**: Refine instead of master. A final variant in between the UR gates and the ON-LSTM’s gates combines cumax with refine gates. In this formulation, as in UR gates, the refine gate modifies the forget gate and the input gate is tied to the effective forget gate. The forget gate is ordered using cumax .

Table 1 summarizes the gating modifications we consider and their naming conventions. Note that we also denote the ON-LSTM method as **OM** for mnemonic ease. Finally, we remark that all methods here are controlled with the same number of parameters as the standard LSTM, aside from OM and UM which use an additional $\frac{1}{2C}$ -fraction parameters where C is the downsize factor on the master gates (Appendix B.4). $C = 1$ unless noted otherwise.

5. Experiments

We first perform full ablations of the gating variants (Section 4.1) on two common benchmarks for testing memory models: synthetic memory tasks and pixel-by-pixel image classification tasks. We then evaluate our main method on important applications for recurrent models including language modeling and reinforcement learning, comparing against baselines from literature where appropriate.

The main claims we evaluate for each gating component are (i) the refine gate is more effective than alternatives (the master gate, or no auxiliary gate), and (ii) UGI is more effective than standard initialization for sigmoid gates. In particular, we expect the *R gate to be more effective than *M or *- for any primary gate *, and we expect U* to be better than -* and comparable to O* for any auxiliary gate *.

The standard LSTM (--) uses forget bias 1.0 (Section

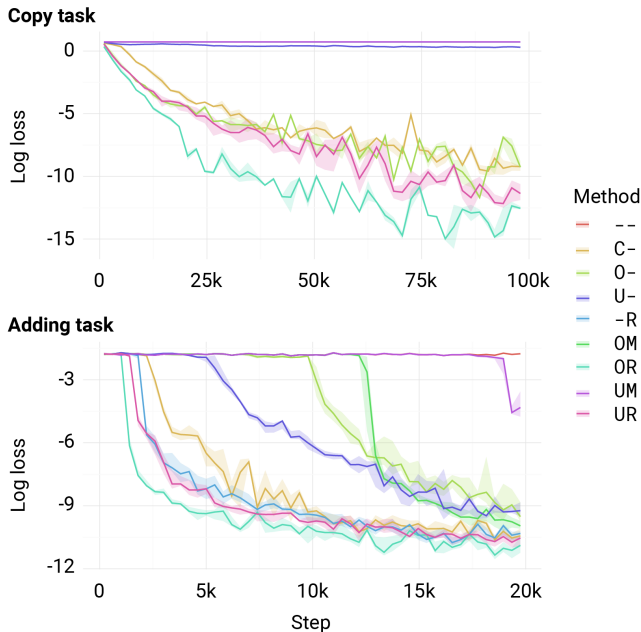


Figure 4. Performance on synthetic memory: Copy task using sequences of length 500. Several methods including standard gates fail to make any progress (overlapping flat curves at baseline). Note that methods that combine the refine gate with a range of gate values (OR, UR) perform best. But the refine gate on its own does not perform well. Adding task using sequences of length 2000. Most methods eventually make progress, but again methods that combine the refine gate with a range of gate values (OR, UR) perform best.

2.2). When chrono initialization is used and not explicitly tuned, we set T_{max} to be proportional to the hidden size. This heuristic uses the intuition that if dependencies of length T exist, then so should dependencies of all lengths $\leq T$. Moreover, the amount of information that can be remembered is proportional to the number of hidden units.

All of our benchmarks have prior work with recurrent baselines, from which we used the same models, protocol, and hyperparameters whenever possible, changing only the gating mechanism without doing any additional tuning for the refine gating mechanisms. Full protocols and details for all experiments are given in Appendix D.

5.1. Synthetic Memory Tasks

Our first set of experiments is on synthetic memory tasks (Hochreiter & Schmidhuber, 1997; Arjovsky et al., 2016) that are known to be hard for standard LSTMs to solve. For these tasks, we used single layer models with 256 hidden units, trained using Adam with learning rate 10^{-3} .

Copy task. The input is a sequence of $N + 20$ digits where the first 10 tokens (a_0, a_1, \dots, a_9) are randomly chosen from $\{1, \dots, 8\}$, the middle N tokens are set to 0, and the last ten tokens are 9. The goal of the recurrent model is to output (a_0, \dots, a_9) in order on the last 10 time steps, whenever the

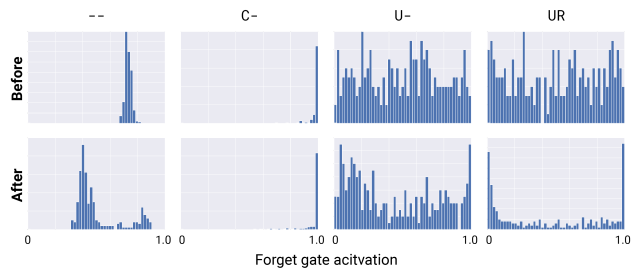


Figure 5. Distribution of forget gate activations before and after training. For the Copy task. We show the distribution of activations f_t for four methods: -- cannot learn large enough f_t and makes no progress on the task. C- initializes with extremal activations which barely change during training. U- makes progress by encouraging a range of forget gate values, but this distribution does not change significantly during training due to saturation. UR starts with the same distribution as U- but is able to learn extreme gate values, which allows it to access the distal inputs, as necessary for this task. Appendix E.1 shows a reverse task where UR is able to un-learn from a saturated regime.

cue token 9 is presented. We trained our models using cross-entropy with baseline loss $\log(8)$ (Appendix D.1).

Adding task. The input consists of two sequences: 1. N numbers (a_0, \dots, a_{N-1}) sampled independently from $\mathcal{U}[0,1]$ 2. an index $i_0 \in [0, N/2)$ and $i_1 \in [N/2, N)$, together encoded as a two-hot sequence. The target output is $a_{i_0} + a_{i_1}$ and models are evaluated by the mean squared error with baseline loss $1/6$.

Figure 4 shows the loss of various methods on the Copy and Adding tasks. The only gate combinations capable of solving Copy completely are OR, UR, O-, and C-. This confirms the mechanism of their gates: these are the only methods capable of producing high enough forget gate values either through the cumax non-linearity, the refine gate, or extremely high forget biases. U- is the only other method able to make progress, but converges slower as it suffers from gate saturation without the refine gate. -- makes no progress. OM and UM also get stuck at the baseline loss, despite OM’s cumax activation, which we hypothesize is due to the suboptimal magnitudes of the gates at initialization (Appendix B.4). On the Adding task, every method besides -- is able to eventually solve it, with all refine gate variants fastest.

Figure 5 shows the distributions of forget gate activations of sigmoid-activation methods, before and after training on the Copy task. It shows that activations near 1.0 are important for a model’s ability to make progress or solve this task, and that adding the refine gate makes this significantly easier.

5.2. Pixel-by-pixel Image Classification

These tasks involve feeding a recurrent model the pixels of an image in a scanline order before producing a classification

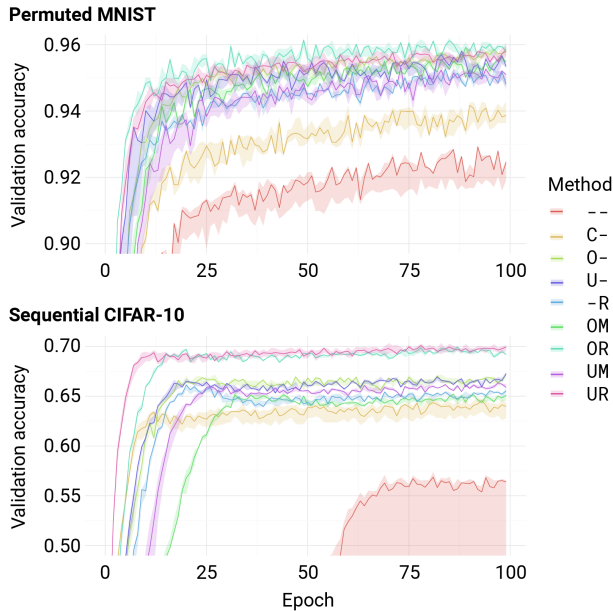


Figure 6. Performance on pixel-by-pixel image classification. Performance is consistent with synthetic tasks. -- performs the worst. Other gating variants improve performance. Note that methods that combine the refine gate with a range of gate values (OR, UR) perform best.

label. We test on the sequential MNIST (sMNIST), permuted MNIST (pMNIST) (Le et al., 2015), and sequential CIFAR-10 (sCIFAR-10) tasks. Each LSTM method was ran with a learning rate sweep with 3 seeds each. We found that many methods were quite unstable, with multiple seeds diverging. Figure 6 shows the accuracy curves of each method at their best *stable* learning rate. The basic LSTM is noticeably worse than all of the others. This suggests that any of the gate modifications, whether better initialization, cumax non-linearity, or master or refine gates, are better than standard gates especially when long-term dependencies are present. Additionally, the uniform gate initialization methods are generally better than the ordered and chrono initialization, and the refine gate performs better than the master gate. Table 2 compares the test accuracy of our main model against other models from the literature. In addition, we tried variants of GRUs and the addition of a generic regularization technique—we chose Zoneout (Krueger et al., 2016) with default hyperparameters ($z_c = 0.5$, $z_h = 0.05$). This combination even outperformed non-recurrent models on sequential MNIST and CIFAR-10.

From Sections 5.1 and 5.2, we draw a few conclusions about the comparative performance of different gate modifications. First, the refine gate is consistently better than comparable master gates. C- solves the synthetic memory tasks but is worse than any other variant outside of those. We find ordered (cumax) gates to be effective, but speed issues prevent us from using them in more complicated tasks. UR gates are consistently among the best performing and most stable.

Table 2. Comparison to prior methods for pixel-by-pixel image classification. Test acc. on pixel-by-pixel image classification benchmarks. Top: Recurrent baselines and variants. Middle: Non-recurrent sequence models with global receptive field. r-LSTM has 2-layers with an auxiliary loss. Bottom: Our methods.

Method	sMNIST	pMNIST	sCIFAR-10
LSTM (ours)	98.9	95.11	63.01
Dilated GRU (Chang et al., 2017)	99.0	94.6	-
IndRNN (Li et al., 2018a)	99.0	96.0	-
r-LSTM (Trinh et al., 2018)	98.4	95.2	72.2
Transformer (Trinh et al., 2018)	98.9	97.9	62.2
Temporal ConvNet (Bai et al., 2018a)	99.0	97.2	-
TrellisNet (Bai et al., 2018b)	99.20	98.13	73.42
URLSTM	99.28	96.96	71.00
URLSTM + Zoneout (Krueger et al., 2016)	99.21	97.58	74.34
URGRU + Zoneout	99.27	96.51	74.4

Table 3. Language modelling results. Perplexities on the WikiText-103 dataset.

Method	Valid	Test
--	34.3	35.8
C-	35.0	36.4
C- $T_{max} = 8$	34.3	36.1
C- $T_{max} = 11$	34.6	35.8
OM	34.0	34.7
U-	33.8	34.9
UR	33.6	34.6

5.3. Language Modeling

We consider word-level language modeling on the WikiText-103 dataset, where (i) the dependency lengths are much shorter than in the synthetic tasks, (ii) language has an implicit hierarchical structure and timescales of varying lengths. We evaluate our gate modifications against the exact hyperparameters of a SOTA LSTM-based baseline (Rae et al., 2018) without additional tuning (Appendix D). Additionally, we compare against ON-LSTM, which was designed for this domain (Shen et al., 2018), and chrono initialization, which addresses dependencies of a particular timescale as opposed to timescale-agnostic UGI methods. In addition to our default hyperparameter-free initialization, we tested models with the chrono hyperparameter T_{max} manually set to 8 and 11, values previously used for language modeling to mimic fixed biases of about 1.0 and 2.0 respectively (Tallec & Ollivier, 2018).

Table 3 shows Validation and Test set perplexities for various models. We find that OM, U-, and UR improve over -- with no additional tuning. However, although OM was designed to capture the hierarchical nature of language with the cumax activation, it does not perform better than U- and UR. Appendix D, Figure 11 additionally shows validation perplexity curves, which indicate that UR overfits less than the other methods.

The chrono initialization using our aforementioned initial-

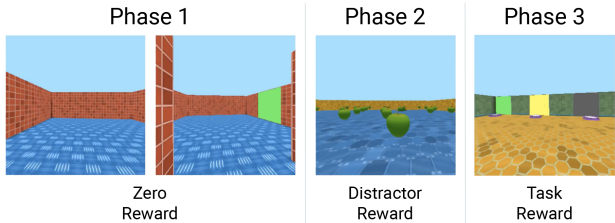


Figure 7. **Active match.** Hung et al. (2018). The agent navigates a 3D world using observations from a first person camera. The task has three phases. In phase 1, the agent must search for a colored cue. In phase 2, the agent is exposed to apples which give distractor rewards. In phase 3, the agent must correctly recall the color of the cue and pick the sensor near the corresponding color to receive the task reward. An episode lasts between 450 and 600 steps, requiring long-term memory and credit assignment.

ization strategy makes biases far too large. While manually tweaking the T_{max} hyperparameter helps, it is still far from any UGI-based methods. We attribute these observations to the nature of language having dependencies on multiple widely-varying timescales, and that UGI is enough to capture these without resorting to strictly enforced hierarchies such as in OM.

5.4. Reinforcement Learning Memory Tasks

In most partially observable reinforcement learning (RL) tasks, the agent can observe only part of the environment at a time and thus requires a memory to summarize what it has seen previously. However, designing memory architectures for reinforcement learning problems has been a challenging task (Oh et al., 2016; Wayne et al., 2018). Many memory architectures for RL use an LSTM component to summarize what an agent has seen.

We investigated if changing the gates of these LSTMs can improve the performance of RL agents, especially on difficult tasks involving memory and long-term credit assignment. We chose the **Passive match** and **Active match** tasks from Hung et al. (2018) using A3C agents (Mnih et al., 2016). See Figure 7 for a description of Active match. Passive match is similar, except the agent always starts facing the colored cue. As a result, Passive Match only tests long term memory, not long-term credit assignment. Only the final task reward is reported.

Hung et al. (2018) evaluated agents with different recurrent cores: basic LSTM, LSTM+Mem (an LSTM with memory), and RMA (which also uses an LSTM core), and found the standard LSTM was not able to solve these tasks. We modified the LSTM agent with our gate mechanisms. Figure 8 shows the results of different methods on the Passive match and Active match tasks with distractors. These tasks are structurally similar to the synthetic tasks (Sec. 5.1) requiring retrieval of a memory over hundreds of steps to solve the

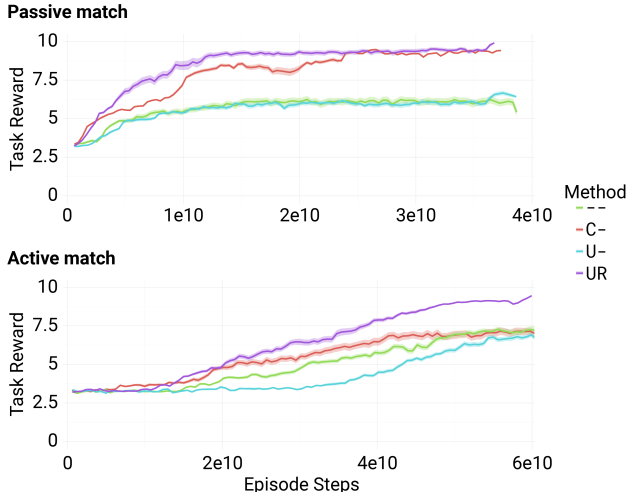


Figure 8. **Performance on reinforcement learning tasks that require memory.** We evaluated the image matching tasks from Hung et al. (2018), which test memorization and credit assignment, using an A3C agent (Mnih et al., 2016) with an LSTM policy core. We observe that general trends from the synthetic tasks (Section (5.1)) transfer to this reinforcement learning setting.

task, and we found that those trends largely transferred to the RL setting even with several additional confounders present such as agents learning via RL algorithms, being required to learn relevant features from pixels rather than being given the relevant tokens, and being required to explore in the Active Match case.

We found that the UR gates substantially improved the performance of the basic LSTM on both Passive Match and Active Match tasks with distractor rewards. The URLSTM was the only method able to get near optimal performance on both tasks, and achieved similar final performance to the LSTM+Mem and RMA agents reported in (Hung et al., 2018).

5.5. Additional Results and Experimental Conclusions

Appendix (E.1) shows an additional synthetic experiment investigating the effect of refine gates on saturation. Appendix (E.3) has results on a program execution task, which is interesting for having explicit long and variable-length dependencies and hierarchical structure. It additionally shows another very different gated recurrent model where the UR gates provide consistent improvement.

Finally, we would like to comment on the longevity of the LSTM, which for example was frequently found to outperform newer competitors when better tuned (Melis et al., 2017; Merity, 2019). Although many improvements have been suggested over the years, none have been proven to be as robust as the LSTM across an enormously diverse range of sequence modeling tasks. By experimentally starting from

well-tuned LSTM baselines, we believe our simple isolated gate modifications to actually be robust improvements. In Appendix B.3 and B.4, we offer a few conclusions for the practitioner about the other gate components considered based on our experimental experience.

6. Discussion

In this work, we introduce and evaluate several modifications to the ubiquitous gating mechanism that appears in recurrent neural networks. We describe methods that improve on the standard gating method by alleviating problems with initialization and optimization. The mechanisms considered include changes on independent axes, namely initialization/activations and auxiliary gates, and we perform extensive ablations on our improvements with previously considered modifications. Our main gate model robustly improves on standard gates across many different tasks and recurrent cores, while requiring less tuning. Finally, we emphasize that these improvements are entirely independent of the large body of research on neural network architectures that use gates, and hope that these insights can be applied to improve machine learning models at large.

References

- Arjovsky, M., Shah, A., and Bengio, Y. Unitary evolution recurrent neural networks. In *International Conference on Machine Learning*, pp. 1120–1128, 2016.
- Bahdanau, D., Cho, K., and Bengio, Y. Neural machine translation by jointly learning to align and translate. *arXiv preprint arXiv:1409.0473*, 2014.
- Bai, S., Kolter, J. Z., and Koltun, V. An empirical evaluation of generic convolutional and recurrent networks for sequence modeling. *arXiv preprint arXiv:1803.01271*, 2018a.
- Bai, S., Kolter, J. Z., and Koltun, V. Trellis networks for sequence modeling. *arXiv preprint arXiv:1810.06682*, 2018b.
- Bengio, Y., Simard, P., Frasconi, P., et al. Learning long-term dependencies with gradient descent is difficult. *IEEE transactions on neural networks*, 5(2):157–166, 1994.
- Chandar, S., Sankar, C., Vorontsov, E., Kahou, S. E., and Bengio, Y. Towards non-saturating recurrent units for modelling long-term dependencies. *arXiv preprint arXiv:1902.06704*, 2019.
- Chang, S., Zhang, Y., Han, W., Yu, M., Guo, X., Tan, W., Cui, X., Witbrock, M., Hasegawa-Johnson, M. A., and Huang, T. S. Dilated recurrent neural networks. In *Advances in Neural Information Processing Systems*, pp. 77–87, 2017.
- Cho, K., Van Merriënboer, B., Gulcehre, C., Bahdanau, D., Bougares, F., Schwenk, H., and Bengio, Y. Learning phrase representations using RNN encoder-decoder for statistical machine translation. *arXiv preprint arXiv:1406.1078*, 2014.
- Chung, J., Gulcehre, C., Cho, K., and Bengio, Y. Empirical evaluation of gated recurrent neural networks on sequence modeling. *arXiv preprint arXiv:1412.3555*, 2014.
- Chung, J., Ahn, S., and Bengio, Y. Hierarchical multiscale recurrent neural networks. *arXiv preprint arXiv:1609.01704*, 2016.
- Dai, Z., Yang, Z., Yang, Y., Cohen, W. W., Carbonell, J., Le, Q. V., and Salakhutdinov, R. Transformer-xl: Attentive language models beyond a fixed-length context. *arXiv preprint arXiv:1901.02860*, 2019.
- Espeholt, L., Soyer, H., Munos, R., Simonyan, K., Mnih, V., Ward, T., Doron, Y., Firoiu, V., Harley, T., Dunning, I., et al. Impala: Scalable distributed deep-rl with importance weighted actor-learner architectures. In *International Conference on Machine Learning*, pp. 1406–1415, 2018.
- Graves, A., Wayne, G., and Danihelka, I. Neural Turing machines. *arXiv preprint arXiv:1410.5401*, 2014.
- Greff, K., Srivastava, R. K., Koutník, J., Steunebrink, B. R., and Schmidhuber, J. LSTM: A search space odyssey. *IEEE transactions on neural networks and learning systems*, 28(10):2222–2232, 2016.
- Gulcehre, C., Moczulski, M., Denil, M., and Bengio, Y. Noisy activation functions. In *International conference on machine learning*, pp. 3059–3068, 2016.
- Gulcehre, C., Chandar, S., and Bengio, Y. Memory augmented neural networks with wormhole connections. *arXiv preprint arXiv:1701.08718*, 2017.
- Henaff, M., Szlam, A., and LeCun, Y. Recurrent orthogonal networks and long-memory tasks. *arXiv preprint arXiv:1602.06662*, 2016.
- Hochreiter, S. Untersuchungen zu dynamischen neuronalen netzen. *Diploma, Technische Universität München*, 91 (1), 1991.
- Hochreiter, S. and Schmidhuber, J. Long short-term memory. *Neural computation*, 9(8):1735–1780, 1997.
- Hochreiter, S., Bengio, Y., Frasconi, P., Schmidhuber, J., et al. Gradient flow in recurrent nets: the difficulty of learning long-term dependencies, 2001.
- Hung, C.-C., Lillicrap, T., Abramson, J., Wu, Y., Mirza, M., Carnevale, F., Ahuja, A., and Wayne, G. Optimizing agent behavior over long time scales by transporting value. *arXiv preprint arXiv:1810.06721*, 2018.

- Jang, E., Gu, S., and Poole, B. Categorical reparameterization with Gumbel-softmax. *arXiv preprint arXiv:1611.01144*, 2016.
- Jozefowicz, R., Zaremba, W., and Sutskever, I. An empirical exploration of recurrent network architectures. In *International Conference on Machine Learning*, pp. 2342–2350, 2015.
- Kapturowski, S., Ostrovski, G., Quan, J., Munos, R., and Dabney, W. Recurrent experience replay in distributed reinforcement learning. In *The International Conference on Learning Representations (ICLR)*, 2018.
- Kingma, D. P. and Ba, J. Adam: A method for stochastic optimization. *arXiv preprint arXiv:1412.6980*, 2014.
- Kočíšký, T., Schwarz, J., Blunsom, P., Dyer, C., Hermann, K. M., Melis, G., and Grefenstette, E. The NarrativeQA reading comprehension challenge. *Transactions of the Association for Computational Linguistics*, 6:317–328, 2018.
- Koutník, J., Greff, K., Gomez, F., and Schmidhuber, J. A clockwork rnn. *arXiv preprint arXiv:1402.3511*, 2014.
- Krueger, D., Maharaj, T., Kramár, J., Pezeshki, M., Ballas, N., Ke, N. R., Goyal, A., Bengio, Y., Courville, A., and Pal, C. Zoneout: Regularizing RNNs by randomly preserving hidden activations. *arXiv preprint arXiv:1606.01305*, 2016.
- Le, Q. V., Jaitly, N., and Hinton, G. E. A simple way to initialize recurrent networks of rectified linear units. *arXiv preprint arXiv:1504.00941*, 2015.
- Li, S., Li, W., Cook, C., Zhu, C., and Gao, Y. Independently recurrent neural network (IndRNN): Building a longer and deeper RNN. In *Proceedings of the IEEE Conference on Computer Vision and Pattern Recognition*, pp. 5457–5466, 2018a.
- Li, Z., He, D., Tian, F., Chen, W., Qin, T., Wang, L., and Liu, T.-Y. Towards binary-valued gates for robust LSTM training. *arXiv preprint arXiv:1806.02988*, 2018b.
- Maddison, C. J., Mnih, A., and Teh, Y. W. The concrete distribution: A continuous relaxation of discrete random variables. *arXiv preprint arXiv:1611.00712*, 2016.
- Melis, G., Dyer, C., and Blunsom, P. On the state of the art of evaluation in neural language models. *arXiv preprint arXiv:1707.05589*, 2017.
- Merity, S. Single headed attention rnn: Stop thinking with your head. *arXiv preprint arXiv:1911.11423*, 2019.
- Merity, S., Xiong, C., Bradbury, J., and Socher, R. Pointer sentinel mixture models. *arXiv preprint arXiv:1609.07843*, 2016.
- Mnih, V., Badia, A. P., Mirza, M., Graves, A., Lillicrap, T., Harley, T., Silver, D., and Kavukcuoglu, K. Asynchronous methods for deep reinforcement learning. In *International conference on machine learning*, pp. 1928–1937, 2016.
- Oh, J., Chockalingam, V., Singh, S., and Lee, H. Control of memory, active perception, and action in Minecraft. *arXiv preprint arXiv:1605.09128*, 2016.
- Radford, A., Wu, J., Child, R., Luan, D., Amodei, D., and Sutskever, I. Language models are unsupervised multitask learners. *OpenAI Blog*, 1(8), 2019.
- Rae, J. W., Dyer, C., Dayan, P., and Lillicrap, T. P. Fast parametric learning with activation memorization. *arXiv preprint arXiv:1803.10049*, 2018.
- Santoro, A., Faulkner, R., Raposo, D., Rae, J., Chrzanowski, M., Weber, T., Wierstra, D., Vinyals, O., Pascanu, R., and Lillicrap, T. Relational recurrent neural networks. In *Advances in Neural Information Processing Systems*, pp. 7299–7310, 2018.
- Shen, Y., Tan, S., Sordoni, A., and Courville, A. Ordered neurons: Integrating tree structures into recurrent neural networks. *arXiv preprint arXiv:1810.09536*, 2018.
- Srivastava, N., Hinton, G., Krizhevsky, A., Sutskever, I., and Salakhutdinov, R. Dropout: a simple way to prevent neural networks from overfitting. *The journal of machine learning research*, 15(1):1929–1958, 2014.
- Tallec, C. and Ollivier, Y. Can recurrent neural networks warp time? *arXiv preprint arXiv:1804.11188*, 2018.
- Trinh, T. H., Dai, A. M., Luong, M.-T., and Le, Q. V. Learning longer-term dependencies in RNNs with auxiliary losses. *arXiv preprint arXiv:1803.00144*, 2018.
- van der Westhuizen, J. and Lasenby, J. The unreasonable effectiveness of the forget gate. *arXiv preprint arXiv:1804.04849*, 2018.
- Wayne, G., Hung, C.-C., Amos, D., Mirza, M., Ahuja, A., Grabska-Barwinska, A., Rae, J., Mirowski, P., Leibo, J. Z., Santoro, A., et al. Unsupervised predictive memory in a goal-directed agent. *arXiv preprint arXiv:1803.10760*, 2018.
- Weston, J., Chopra, S., and Bordes, A. Memory networks. *arXiv preprint arXiv:1410.3916*, 2014.
- Zaremba, W. and Sutskever, I. Learning to execute. *arXiv preprint arXiv:1410.4615*, 2014.
- Zilly, J. G., Srivastava, R. K., Koutník, J., and Schmidhuber, J. Recurrent highway networks. In *Proceedings of the 34th International Conference on Machine Learning-Volume 70*, pp. 4189–4198. JMLR. org, 2017.

A. Pseudocode

We show how the gated update in a typical LSTM implementation can be easily replaced by UR- gates.

The following snippets show pseudocode for the the gated state updates for a vanilla LSTM model (top) and UR-LSTM (bottom).

```
forget_bias = 1.0 # hyperparameter
...
f, i, u, o = Linear(x, prev_hidden)
f_ = sigmoid(f + forget_bias)
i_ = sigmoid(i)
next_cell = f_ * prev_cell + i_ * tanh(u)
next_hidden = sigmoid(o) * tanh(next_cell)
```

Listing 1: LSTM

```
# Initialization
u = np.random.uniform(low=1/hidden_size,
                      high=1-1/hidden_size,
                      size=hidden_size)
forget_bias = -np.log(1/u-1)
...
# Recurrent update
f, r, u, o = Linear(x, prev_hidden)
f_ = sigmoid(f + forget_bias)
r_ = sigmoid(r - forget_bias)
g = 2*r_*f_ + (1-2*r_)*f_**2
next_cell = g * prev_cell + (1-g) * tanh(u)
next_hidden = sigmoid(o) * tanh(next_cell)
```

Listing 2: UR-LSTM

B. Further discussion on related methods

Section 4 briefly introduced chrono initialization (Tallec & Ollivier, 2018) and the ON-LSTM (Shen et al., 2018), closely related methods that modify the gating mechanism of LSTMs. We provide more detailed discussion on these in Sections B.3 and B.4 respectively. Section B.1 has a more thorough overview of related work on recurrent neural networks that address long-term dependencies or saturating gates.

B.1. Related Work

Several methods exist for addressing gate saturation or allowing more binary activations. Gulcehre et al. (2016) proposed to use piece-wise linear functions with noise in order to allow the gates to operate in saturated regimes. Li et al. (2018b) instead use the Gumbel trick (Maddison et al., 2016; Jang et al., 2016), a technique for learning discrete variables within a neural network, to train LSTM models with discrete gates. These stochastic approaches can suffer from issues such as gradient estimation bias, unstable training, and limited expressivity

from discrete instead of continuous gates. Additionally they require more involved training protocols with an additional temperature hyperparameter that needs to be tuned explicitly.

Alternatively, gates can be removed entirely if strong constraints are imposed on other parts of the model. (Li et al., 2018a) use diagonal weight matrices and require stacked RNN layers to combine information between hidden units. A long line of work has investigated the use of identity or orthogonal initializations and constraints on the recurrent weights to control multiplicative gradients unrolled through time (Le et al., 2015; Arjovsky et al., 2016; Henaff et al., 2016). (Chandar et al., 2019) proposed another RNN architecture using additive state updates and non-saturating activation functions instead of gates. However, although these gate-less techniques can be used to alleviate the vanishing gradient problem with RNNs, unbounded activation functions can cause less stable learning dynamics and exploding gradients.

As mentioned, a particular consequence of the inability of gates to approach extrema is that gated recurrent models struggle to capture very long dependencies. These problems have traditionally been addressed by introducing new components to the basic RNN setup. Some techniques include stacking layers in a hierarchy (Chung et al., 2016), adding skip connections and dilations (Koutnik et al., 2014; Chang et al., 2017), using an external memory (Graves et al., 2014; Weston et al., 2014; Wayne et al., 2018; Gulcehre et al., 2017), auxiliary semi-supervision (Trinh et al., 2018), and more. However, these approaches have not been widely adopted over the standard LSTM as they are often specialized for certain tasks, are not as robust, and introduce additional complexity. Recently the transformer model has been successful in many applications areas such as NLP (Radford et al., 2019; Dai et al., 2019). However, recurrent neural networks are still important and commonly used due their faster inference without the need to maintain the entire sequence in memory. We emphasize that the vast majority of proposed RNN changes are completely orthogonal to the simple gate improvements in this work, and we do not focus on them.

A few other recurrent cores that use the basic gated update (1) but use more sophisticated update functions u include the GRU, Reconstructive Memory Agent (RMA; Hung et al., 2018), and Relational Memory Core (RMC; Santoro et al., 2018), which we consider in our experiments.

B.2. Effect of proposed methods on timescales

We briefly review the connection between our methods and the effective timescales that gated RNNs capture. Recall that Section 3.2 defines the *characteristic timescale* of a neuron with forget activation f_t as $1/(1-f_t)$, which would be the number of timesteps it takes to decay that neuron by a constant.

The fundamental principle of gated RNNs is that the activations of the gates affects the timescales that the model can address; for example, forget gate activations near 1.0 are necessary to capture long-term dependencies.

Thus, although our methods were defined in terms of activations g_t , it is illustrative to reason with their characteristic timescales $1/(1-g_t)$ instead, whence both UGI and refine gate also have clean interpretations.

First, UGI is equivalent to initializing the decay period from a particular heavy-tailed distribution, in contrast to standard initialization with a fixed decay period $(1-\sigma(b_f))^{-1}$.

Proposition 1. *UGI is equivalent to sampling the decay period $D = 1/(1-f_t)$ from a distribution with density proportional to $\mathbb{P}(D = x) \propto \frac{d}{dx}(1-1/x) = x^{-2}$, i.e. a Pareto($\alpha=2$) distribution.*

On the other hand, for any forget gate activation f_t with timescale $D = 1/(1-f_t)$, the refine gate fine-tunes it between $D = 1/(1-f_t^2) = 1/(1-f_t)(1+f_t)$ and $1/(1-f_t)^2$.

Proposition 2. *Given a forget gate activation with timescale D , the refine gate creates an effective forget gate with timescale in $(D/2, D^2)$.*

B.3. Chrono Initialization

The chrono initialization

$$b_f \sim \log(\mathcal{U}([1, T_{max}-1])) \quad (14)$$

$$b_i = -b_f. \quad (15)$$

was the first to explicitly attempt to initialize the activation of gates across a distributional range. It was motivated by matching the gate activations to the desired timescales.

They also elucidate the benefits of tying the input and forget gates, leading to the simple trick (15) for approximating tying the gates at initialization, which we borrow for UGI. (We remark that perfect tied initialization can be accomplished by fully tying the linear maps $\mathcal{L}_f, \mathcal{L}_i$, but (15) is a good approximation.)

However, the main drawback of CI is that the initialization distribution is too heavily biased toward large terms. This leads to empirical consequences such as difficult tuning (due to most units starting in the saturation regime, requiring different learning rates) and high sensitivity to the hyperparameter T_{max} that represents the maximum potential length of dependencies. For example, Tallec & Ollivier (2018) set this parameter according to a different protocol for every task, with values ranging from 8 to 2000. Our experiments used a hyperparameter-free method to initialize T_{max} (Section 5), and we found that chrono initialization generally severely over-emphasizes long-term dependencies if T_{max} is not carefully controlled.

A different workaround suggested by Tallec & Ollivier (2018) is to sample from $\mathbb{P}(T=k) \propto \frac{1}{k \log^2(k+1)}$ and setting $b_f = \log(T)$. Note that such an initialization would be almost equivalent to sampling the decay period from the distribution with density $\mathbb{P}(D=x) \propto (x \log^2 x)^{-1}$ (since the decay period is $(1-f)^{-1} = 1 + \exp(b_f)$). This parameter-free initialization is thus similar in spirit to the uniform gate initialization (Proposition 1), but from a much heavier-tailed distribution that emphasizes very long-term dependencies.

These interpretations suggest that it is plausible to define a family of Pareto-like distributions from which to draw the initial decay periods from, with this distribution treated as a hyperparameter. However, with no additional prior information on the task, we believe the uniform gate initialization to be the best candidate, as it 1. is a simple distribution with easy implementation, 2. has characteristic timescale distributed as an intermediate balance between the heavy-tailed chrono initialization and sharply decaying standard initialization, and 3. is similar to the ON-LSTM’s cumax activation, in particular matching the initialization distribution of the cumax activation.

Table 4 summarizes the decay period distributions at initialization using different activations and initialization strategies.

In general, our experimental recommendation for CI is that it can be better than standard initialization or UGI when certain conditions are met (tasks with long dependencies and nearly fixed-length sequences as in Sections 5.1, 5.4) and/or when it can be explicitly tuned (both the hyperparameter T_{max} , as well as the learning rate to compensate for almost all units starting in saturation). Otherwise, we recommend UGI or standard initialization. We found no scenarios where it outperformed UR- gates.

B.4. ON-LSTM

In this section we elaborate on the connection between the mechanism of (Shen et al., 2018) and our methods. We define the full ON-LSTM and show how its gating mechanisms can be improved. For example, there is a remarkable connection between its master gates and our refine gates – independently of the derivation of refine gates in Section 3.4, we show how a specific way of fixing the normalization of master gates becomes equivalent to a single refine gate.

First, we formally define the full ON-LSTM. The master gates are a cumax-activation gate

$$\tilde{f}_t = \text{cumax}(\mathcal{L}_{\tilde{f}}(x_t, h_{t-1})) \quad (16)$$

$$\tilde{i}_t = 1 - \text{cumax}(\mathcal{L}_{\tilde{i}}(x_t, h_{t-1})). \quad (17)$$

These combine with an independent pair of forget and input gates f_t, i_t , meant to control fine-grained behavior, to create an effective forget/input gate \hat{f}_t, \hat{i}_t which are used to update

Table 4. Distribution of the decay period $D = (1 - f)^{-1}$ using different initialization strategies.

Initialization method	Timescale distribution
Constant bias $b_f = b$	$\mathbb{P}(D = x) \propto \mathbf{1}\{x = 1 + e^b\}$
Chrono initialization (known timescale T_{max})	$\mathbb{P}(D = x) \propto \mathbf{1}\{x \in [2, T_{max}]\}$
Chrono initialization (unknown timescale)	$\mathbb{P}(D = x) \propto \frac{1}{x \log^2 x}$
Uniform gate initialization	$\mathbb{P}(D = x) \propto \frac{1}{x^2}$
cumax activation	$\mathbb{P}(D = x) \propto \frac{1}{x^2}$

the state (equation (1) or (5)).

$$\omega_t = \tilde{f}_t \circ \tilde{i}_t \quad (18)$$

$$\hat{f}_t = f_t \circ \omega_t + (\tilde{f}_t - \omega_t) \quad (19)$$

$$\hat{i}_t = i_t \circ \omega_t + (\tilde{i}_t - \omega_t). \quad (20)$$

As mentioned in Section B.1, this model modifies the standard forget/input gates in two main ways, namely ordering the gates via the cumax activation, and supplying an auxiliary set of gates controlling fine-grained behavior. Both of these are important novelties and together allow recurrent models to better capture tree structures.

However, the UGI and refine gate can be viewed as improvements over each of these, respectively, demonstrated both theoretically (below) and empirically (Sections 5 and E.3), even on tasks involving hierarchical sequences.

Ordered gates Despite having the same parameter count and asymptotic efficiency as standard sigmoid gates, cumax gates seem noticeably slower and less stable in practice for large hidden sizes. Additionally, using auxiliary master gates creates additional parameters compared to the basic LSTM. Shen et al. (2018) alleviated both of these problems by defining a *downsize* operation, whereby neurons are grouped in chunks of size C , each of which share the same master gate values. However, this also creates an additional hyperparameter.

The speed and stability issues can be fixed by just using the sigmoid non-linearity instead of cumax. To recover the most important properties of the cumax—activations at multiple timescales—the equivalent sigmoid gate can be initialized so as to match the distribution of cumax gates at initialization. This is just uniform gate initialization (equation (12)).

However, we believe that the cumax activation is still valuable in many situations if speed and instability are not issues. These include when the hidden size is small, when extremal gate activations are desired, or when ordering needs to be strictly enforced to induce explicit hierarchical structure. For example, Section (5.1) shows that they can solve hard memory tasks by themselves.

Master gates We observe that the magnitudes of master gates are suboptimally normalized. A nice interpretation of gated recurrent models shows that they are a discretization of a continuous differential equation. This leads to the leaky RNN model $h_{t+1} = (1 - \alpha)h_t + \alpha u_t$, where u_t is the update to the model such as $\tanh(W_x x_t + W_h h_t + b)$. Learning α as a function of the current time step leads to the simplest gated recurrent model⁵

$$\begin{aligned} f_t &= \sigma(\mathcal{L}_f(x_t, h_{t-1})) \\ u_t &= \tanh(\mathcal{L}_u(x_t, h_{t-1})) \\ h_t &= f_t h_{t-1} + (1 - f_t) u_t. \end{aligned}$$

Tallec & Ollivier (2018) show that this exactly corresponds to the discretization of a differential equation that is invariant to *time warpings* and time rescalings. In the context of the LSTM, this interpretation requires the values of the forget and input gates to be tied so that $f_t + i_t = 1$. This weight-tying is often enforced, for example in the most popular LSTM variant, the GRU (Cho et al., 2014), or our UR-gates. In a large-scale LSTM architecture search, it was found that removing the input gate was not significantly detrimental (Greff et al., 2016).

However, the ON-LSTM does not satisfy this conventional wisdom that the input and forget gates should sum to close to 1.

Proposition 3. *At initialization, the expected value of the average effective forget gate activation \hat{f}_t is 5/6.*

Let us consider the sum of the effective forget and input gates at initialization. Adding equations (19) and (20) yields

$$\begin{aligned} \hat{f}_t + \hat{i}_t &= (f_t + i_t) \circ \omega_t + (\tilde{f}_t + \tilde{i}_t - 2\omega_t) \\ &= \tilde{f}_t + \tilde{i}_t + (f_t + i_t - 2) \circ \omega_t. \end{aligned}$$

Note that the master gates (16), (17) sum 1 in expectation at initialization, as do the original forget and input gates. Looking at individual units in the ordered master gates, we

⁵In the literature, this is called the JANET (van der Westhuizen & Lasenby, 2018), which is also equivalent to the GRU without a reset gate (Chung et al., 2014), or a recurrent highway network with depth $L = 1$ (Zilly et al., 2017).

have $\mathbb{E}\hat{f}^{(j)} = \frac{j}{n}, \mathbb{E}\hat{i}^{(j)} = 1 - \frac{j}{n}$. Thus the above simplifies to

$$\begin{aligned}\mathbb{E}[\hat{f}_t + \hat{i}_t] &= 1 - \mathbb{E}\omega_t \\ \mathbb{E}[\hat{f}_t^{(j)} + \hat{i}_t^{(j)}] &= 1 - \frac{j}{n} \left(1 - \frac{j}{n}\right) \\ \mathbb{E}\left[\mathbb{E}_{j \in [n]} \hat{f}_t^{(j)} + \hat{i}_t^{(j)}\right] &\approx 1 - \int_0^1 x dx + \int_0^1 x^2 dx \\ &= \frac{5}{6}.\end{aligned}$$

The gate normalization can be fixed by re-scaling equations (19) and (20). It turns out that tying the master gates and re-scaling is exactly equivalent to the mechanism of a refine gate. In this equivalence, the role of the master and forget gates of the ON-LSTM are played by our forget and refine gate respectively.

Proposition 4. *Suppose the master gates \tilde{f}_t, \tilde{i}_t are tied and the equations (19)-(20) defining the effective gates \hat{f}_t, \hat{i}_t are rescaled such as to ensure $\mathbb{E}[\hat{f}_t + \hat{i}_t] = 1$ at initialization. The resulting gate mechanism is exactly equivalent to that of the refine gate.*

Consider the following set of equations where the master gates are tied ($\tilde{f}_t + \tilde{i}_t = 1, f_t + i_t = 1$) and (19)-(20) are modified with an extra coefficient (rescaling in bold):

$$\tilde{i}_t = 1 - \tilde{f}_t \quad (21)$$

$$\omega_t = \tilde{f}_t \cdot \tilde{i}_t \quad (22)$$

$$\hat{f}_t = \mathbf{2} \cdot f_t \cdot \omega_t + (\tilde{f}_t - \omega_t) \quad (23)$$

$$\hat{i}_t = \mathbf{2} \cdot i_t \cdot \omega_t + (\tilde{i}_t - \omega_t) \quad (24)$$

Now we have

$$\begin{aligned}\hat{f}_t + \hat{i}_t &= \tilde{f}_t + \tilde{i}_t + 2(f_t + i_t - 1) \cdot \omega_t \\ &= 1 + 2(f_t + i_t - 1) \cdot \omega_t\end{aligned}$$

which has the correct scaling, i.e. $\mathbb{E}[\hat{f}_t + \hat{i}_t] = 1$ at initialization assuming that $\mathbb{E}[f_t + i_t] = 1$ at initialization.

But (23) can be rewritten as follows:

$$\begin{aligned}\hat{f} &= \mathbf{2} \cdot f \cdot \omega + (\tilde{f} - \omega) \\ &= \mathbf{2} \cdot f \cdot \tilde{f} \cdot (1 - \tilde{f}) + (\tilde{f} - \tilde{f} \cdot (1 - \tilde{f})) \\ &= \mathbf{2} f \cdot \tilde{f} - \mathbf{2} f \cdot \tilde{f}^2 + \tilde{f}^2 \\ &= f \cdot \mathbf{2} \tilde{f} - f \cdot \tilde{f}^2 - f \cdot \tilde{f}^2 + \tilde{f}^2 \\ &= f \cdot (1 - (1 - \tilde{f}))^2 + (1 - f) \cdot \tilde{f}^2.\end{aligned}$$

This is equivalent to the refine gate, where the master gate plays the role of the forget gate and the forget gate plays the role of the refine gate. It can be shown that in this case, the

effective input gate \hat{i}_t (24) is also defined through a refine gate mechanism, where $\tilde{i}_t = 1 - \tilde{f}_t$ is refined by i_t :

$$\hat{i} = i \cdot (1 - (1 - \tilde{i}))^2 + (1 - i) \cdot \tilde{i}^2.$$

Based on our experimental findings, in general we would recommend the refine gate in place of the master gate.

B.5. Gate ablation details

For clarity, we formally define the gate ablations considered which mix and match different gate components.

We remark that other combinations are possible, for example combining CI with either auxiliary gate type, which would lead to CR- or CM- gates. Alternatively, the master or refine gates could be defined using different activation and initialization strategies. We chose not to consider these methods due to lack of interpretation and theoretical soundness.

O- This ablation uses the cumax activation to order the forget/input gates and has no auxiliary gates.

$$f_t = \text{cumax}(\mathcal{L}_f(x_t, h_{t-1})) \quad (25)$$

$$i_t = 1 - \text{cumax}(\mathcal{L}_i(x_t, h_{t-1})). \quad (26)$$

We note that one difficulty with this in practice is the reliance on the expensive cumax, and hypothesize that this is perhaps the ON-LSTM's original motivation for the second set of gates combined with downsizing.

UM- This variant of the ON-LSTM ablates the cumax operation on the master gates, replacing it with a sigmoid activation initialized with UGI. Equations (16), (17) are replaced with

$$u = \mathcal{U}(0, 1) \quad (27)$$

$$b_f = \sigma^{-1}(u) \quad (28)$$

$$\tilde{f}_t = \sigma(\mathcal{L}_{\tilde{f}}(x_t, h_{t-1}) + b_f) \quad (29)$$

$$\tilde{i}_t = \sigma(\mathcal{L}_{\tilde{i}}(x_t, h_{t-1}) - b_f) \quad (30)$$

Equations (18)-(20) are then used to define effective gates \hat{f}_t, \hat{i}_t which are used in the gated update (1) or (5).

OR- This ablation combines ordered main gates with an auxiliary refine gate.

$$\tilde{f}_t = \text{cumax}(\mathcal{L}_{\tilde{f}}(x_t, h_{t-1}) + b_f) \quad (31)$$

$$r_t = \sigma(\mathcal{L}_r(x_t, h_{t-1}) + b_r) \quad (32)$$

$$g_t = r_t \cdot (1 - (1 - f_t)^2) + (1 - r_t) \cdot f_t^2 \quad (33)$$

$$i_t = 1 - g_t \quad (34)$$

g_t, i_t are used as the effective forget and input gates.

C. Analysis Details

The gradient analysis in Figure 3 was constructed as follows. Let f, r, g be the forget, refine, and effective gates

$$g = 2rf + (1 - 2r)f^2.$$

Letting x, y be the pre-activations of the sigmoids on f and r , the gradient of g can be calculated as

$$\begin{aligned}\nabla_x g &= 2rf(1-f) + (1-2r)(2f)(f(1-f)) \\ &= 2f(1-f)[r + (1-2r)f]\end{aligned}$$

$$\nabla_y g = 2fr(1-r) + (-2f^2)r(1-r) = 2fr(1-r)(1-f)$$

$$\|\nabla g\|^2 = [2f(1-f)]^2 [(r+f-2fr)^2 + r^2(1-r)^2].$$

Substituting the relation

$$r = \frac{g - f^2}{2f(1-f)},$$

this reduces to the Equation 35,

$$\begin{aligned}\|\nabla g\|^2 &= ((g - f^2)(1 - 2f) + 2f^2(1 - f))^2 \\ &\quad + (g - f^2)^2 \left(1 - \frac{g - f^2}{2f(1-f)}\right)^2.\end{aligned}\quad (35)$$

Given the constraint $f^2 \leq g \leq 1 - (1 - f)^2$, this function can be minimized and maximized in terms of g to produce the upper and lower bounds in Figure 3b. This was performed numerically.

D. Experimental Details

To normalize the number of parameters used for models using master gates, i.e. the OM- and UM- gating mechanisms, we used a downsize factor on the main gates (see Section B.4). This was set to $C = 16$ for the synthetic and image classification tasks, and $C = 32$ for the language modeling and program execution tasks which used larger hidden sizes.

D.1. Synthetic Tasks

All models consisted of single layer LSTMs with 256 hidden units, trained with the Adam optimizer (Kingma & Ba, 2014) with learning rate $1e-3$. Gradients were clipped at 1.0.

The training data consisted of randomly generated sequences for every minibatch rather than iterating through a fixed dataset. Each method ran 3 seeds, with the same training data for every method.

Our version of the Copy task is a very minor variant of other versions reported in the literature, with the main difference being that the loss is considered only over the last 10 output tokens which need to be memorized. This normalizes the loss so that losses approaching 0 indicate true progress. In

contrast, this task is usually defined with the model being required to output a dummy token at the first $N + 10$ steps, meaning it can be hard to evaluate performance since low average losses simply indicate that the model learns to output the dummy token.

For Figure 4, the log loss curves show the median of 3 seeds, and the error bars indicate 60% confidence.

For Figure 5, each histogram represents the distribution of forget gate values of the hidden units (of which there are 256). The values are created by averaging units over time and samples, i.e., reducing a minibatch of forget gate activations of shape (batch size, sequence length, hidden size) over the first two dimensions, to produce the average activation value for every unit.

D.2. Image Classification

All models used a single hidden layer recurrent network (LSTM or GRU). Inputs x to the model were given in batches as a sequence of shape (sequence length, num channels), (e.g. (1024,3) for CIFAR-10), by flattening the input image left-to-right, top-to-bottom. The outputs of the model of shape (sequence length, hidden size) were processed independently with a single ReLU hidden layer of size 256 before the final fully-connected layer outputting softmax logits. All training was performed with the Adam optimizer, batch size 50, and gradients clipped at 1.0. MNIST trained for 150 epochs, CIFAR-10 used 100 epochs over the training set.

Table 5 All models (LSTM and GRU) used hidden state size 512. Learning rate swept in $\{2e-4, 5e-4, 1e-3, 2e-3\}$ with three seeds each.

Table 5 reports the highest validation score found. The GRU model swept over learning rates $\{2e-4, 5e-4\}$; all methods were unstable at higher learning rates.

Figure 6 shows the median validation accuracy with quartiles (25/75% confidence intervals) over the seeds, for the best-performing stable learning rate (i.e. the one with highest average validation score on the final epoch). This was generally $5e-4$ or $1e-3$, with refine gate variants tending to allow higher learning rates.

Table 2 The UR-LSTM and UR-GRU used 1024 hidden units for the sequential and permuted MNIST task, and 2048 hidden units for the sequential CIFAR task. The vanilla LSTM baseline used 512 hidden units for MNIST and 1024 for CIFAR. Larger hidden sizes were found to be unstable.

Zoneout parameters were fixed to reasonable default settings based on Krueger et al. (2016), which are $z_c = 0.5, z_h = 0.05$ for LSTM and $z = 0.1$ for GRU. When zoneout was used, standard Dropout (Srivastava et al., 2014) with probability

Table 5. Gate ablations on pixel-by-pixel image classification. Validation accuracies on pixel image classification. Asterisks denote divergent runs at the learning rate the best validation score was found at.

Gating Method	-	C-	O-	U-	R-	OM-	OR-	UM-	UR-
pMNIST	94.77**	94.69	96.17	96.05	95.84*	95.98	96.40	95.50	96.43
sCIFAR	63.24**	65.60	67.78	67.63	71.85*	67.73*	70.41	67.29*	71.05
sCIFAR (GRU)	71.30*	64.61	69.81**	70.10	70.74*	70.20*	71.40**	69.17*	71.04

0.5 was also applied to the output classification hidden layer.

D.3. Language Modeling

Hyperparameters are taken from Rae et al. (2018) tuned for the vanilla LSTM, which consist of (chosen parameter bolded out of sweep): {1, 2} LSTM layer, {0.0, 0.1, 0.2, **0.3**} embedding dropout, {yes, **no**} layer norm, and {**shared**, not shared} input/output embedding parameters. Our only divergence is using a hidden size of 3072 instead of 2048, which we found improved the performance of the vanilla LSTM. Training was performed with Adam at learning rate 1e-3, gradients clipped to 0.1, sequence length 128, and batch size 128 on TPU. The LSTM state was reset between article boundaries.

Figure 11 shows smoothed validation perplexity curves showing the 95% confidence intervals over the last 1% of data.

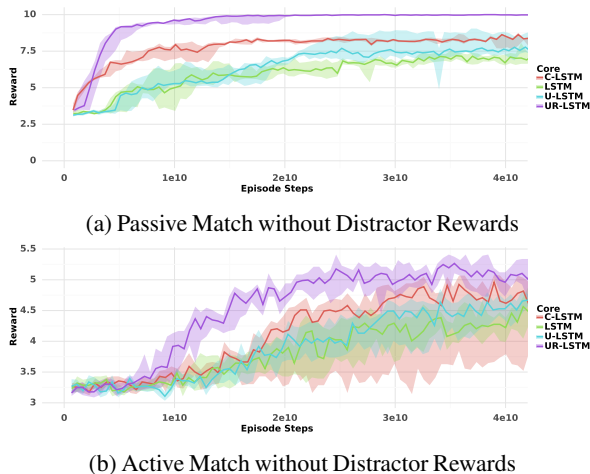


Figure 9. Performance on Reinforcement Learning Tasks that Require Memory. We evaluated the image matching tasks from Hung et al. (2018), which test memorization and credit assignment, using an A3C agent (Mnih et al., 2016) with an LSTM policy core. We observe that general trends from the synthetic tasks (Section (5.1)) transfer to this reinforcement learning setting.

Reinforcement Learning The Active Match and Passive Match tasks were borrowed from Hung et al. (2018) with the same settings. For Figures 9 and 13, the discount factor in the environment was set to $\gamma = .96$. For Figure 10, the discount factor was $\gamma = .998$. Figure 13 corresponds to the full Active

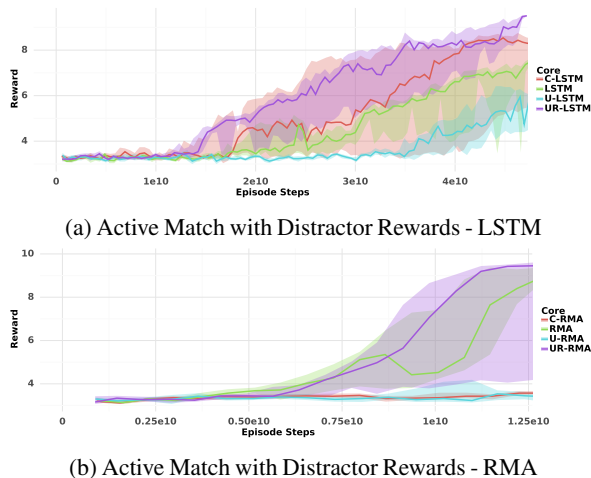


Figure 10. The addition of distractor rewards changes the task and relative performance of different gating mechanisms. For both LSTM and RMA recurrent cores, the UR- gates still perform best.

Match task in Hung et al. (2018), while Figure 10 is their version with small distractor rewards where the apples in the distractor phase give 1 instead of 5 reward.

Figure 8 used 5 seeds per method.

D.4. Program Evaluation

Protocol was taken from Santoro et al. (2018) with minor changes to the hyperparameter search. All models were trained with the Adam optimizer, the *Mix* curriculum strategy from Zaremba & Sutskever (2014), and batch size 128.

RMC: The RMC models used a fixed memory slot size of 512 and swept over {2, 4} memories and {2, 4} attention heads for a total memory size of 1024 or 2048. They were trained for 2e5 iterations.

LSTM: Instead of two-layer LSTMs with sweeps over skip connections and output concatenation, single-layer LSTMs of size 1024 or 2048 were used. Learning rate was swept in {5e-4, 1e-3}, and models were trained for 5e5 iterations. Note that training was still faster than the RMC models despite the greater number of iterations.

D.5. Additional Details

Implementation Details The inverse sigmoid function (12) can be unstable if the input is too close to $\{0, 1\}$. Uniform gate initialization was instead implemented by sampling from the distribution $\mathcal{U}[1/d, 1 - 1/d]$ instead of $\mathcal{U}[0, 1]$, where d is the hidden size, to avoid any potential numerical edge cases. This choice is justified by the fact that with perfect uniform sampling, the expected smallest and largest samples would be $1/(d+1)$ and $1 - 1/(d+1)$.

For distributional initialization strategies, a trainable bias vector was sampled independently from the chosen distribution (i.e. equation (14) or (12)) and added/subtracted to the forget and input gate ((2)-(3)) before the non-linearity. Additionally, each linear model such as $W_{xf}x_t + W_{hf}h_{t-1}$ had its own trainable bias vector, effectively doubling the learning rate on the pre-activation bias terms on the forget and input gates. This was an artifact of implementation and not intended to affect performance.

The refine gate update equation (10) can instead be implemented as

$$\begin{aligned} g_t &= r_t \cdot (1 - (1 - f_t)^2) + (1 - r_t) \cdot f_t^2 \\ &= 2r_t \cdot f_t + (1 - 2r_t) \cdot f_t^2 \end{aligned}$$

Permuted image classification In an effort to standardize the permutation used in the Permuted MNIST benchmark, we use a particular deterministic permutation rather than a random one. After flattening the input image into a one-dimensional sequence, we apply the *bit reversal* permutation. This permutation sends the index i to the index j such that j 's binary representation is the reverse of i 's binary representation. The intuition is that if two indices i, i' are close, they must differ in their lower-order bits. Then the bit-reversed indices will be far apart. Therefore the bit-reversal permutation destroys spatial and temporal locality, which is desirable for these sequence classification tasks meant to test long-range dependencies rather than local structure.

```
def bitreversal_po2(n):
    m = int(math.log(n) / math.log(2))
    perm = np.arange(n).reshape(n, 1)
    for i in range(m):
        n1 = perm.shape[0] // 2
        perm = np.hstack((perm[:n1], perm[n1:]))
    return perm.squeeze(0)

def bitreversal_permutation(n):
    m = int(math.ceil(math.log(n) / math.log(2)))
    N = 1 << m
    perm = bitreversal_po2(N)
    return np.extract(perm < n, perm)
```

Listing 3: Bit-reversal permutation for permuted MNIST.

E. Additional Experiments

E.1. Synthetic Forgetting

Figure 5 on the Copy task demonstrates that extremal gate activations are necessary to solve the task, and initializing the activations near 1.0 is helpful.

This raises the question: what happens if the initialization distribution does not match the task at hand; could the gates learn back to a more moderate regime? We point out that such a phenomenon could occur non-pathologically on more complex setups, such as a scenario where a model trains to remember on a Copy-like task and then needs to “unlearn” as part of a meta-learning or continual learning setup.

Here, we consider such a synthetic scenario and experimentally show that the addition of a refine gate helps models train much faster while in a saturated regime with extremal activations. We also point to the poor performance of C- outside of synthetic memory tasks when using our high hyperparameter-free initialization as more evidence that it is very difficult for standard gates to unlearn undesired saturated behavior.

For this experiment, we initialize the biases of the gates extremely high (effective forget activation $\approx \sigma(6)$). We then consider the Adding task (Section 5.1) of length 500, hidden size 64, learning rate 1e-4. The R-LSTM is able to solve the task, while the LSTM is stuck after 1e4 iterations.

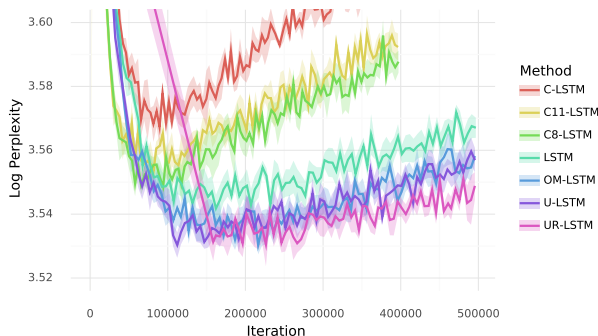


Figure 11. Validation learning curves, illustrating training speed and generalization (i.e. overfitting) behavior.

E.2. Reinforcement Learning

Figures 9 and 10 evaluated our gating methods with the LSTM and RMA models on the Passive Match and Active Match tasks, with and without distractors. We additionally ran the agents on an even harder version of the Active Match task with larger distractor rewards (the full Active Match from Hung et al. (2018)). Learning curves are shown in Figure 13. Similarly to the other results, the UR-gated core is noticeably better than the others. For the DNC model, it is the only one that performs better than random chance.

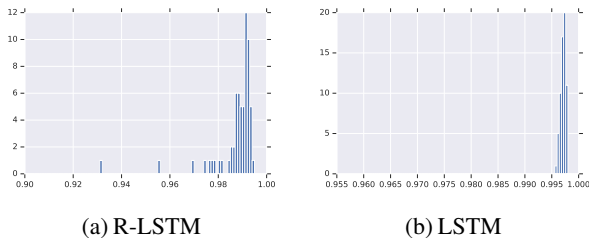


Figure 12. Distribution of forget gate activations after extremal initialization, and training on the Adding task. The UR-LSTM is able to learn much faster in this saturated gate regime while the LSTM does not solve the task. The smallest forget unit for the UR-LSTM after training has characteristic timescale over an order of magnitude smaller than that of the LSTM.

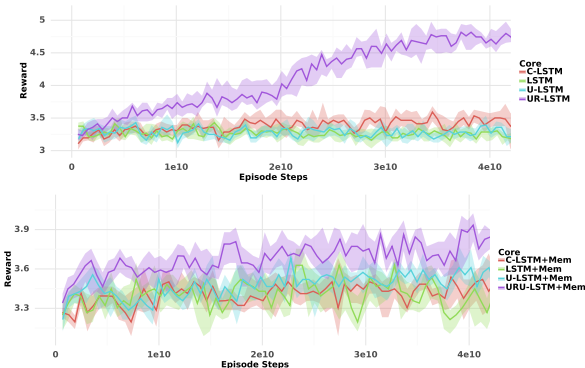


Figure 13. The full Active Match task with large distractor rewards, using agents with LSTM or DNC recurrent cores.

E.3. Program Execution

The Learning to Execute (Zaremba & Sutskever, 2014) dataset consists of algorithmic snippets from a programming language of pseudo-code. An input is a program from this language presented one character at a time, and the target output is a numeric sequence of characters representing the execution output of the program. There are three categories of tasks: Addition, Control, and Program, with distinctive types of input programs. We use the most difficult setting from Zaremba & Sutskever (2014), which uses the parameters $nesting=4$, $length=9$, referring to the nesting depth of control structure and base length of numeric literals, respectively. Examples of input programs are shown in previous works (Zaremba & Sutskever, 2014; Santoro et al., 2018).

We are interested in this task for several reasons. First, we are interested in comparing against the C- and OM- gate methods, because

- The maximum sequence length is fairly long (several hundred tokens), meaning our T_{max} heuristic for C- gates is within the right order of magnitude of dependency lengths.

- The task has highly variable sequence lengths, wherein the standard training procedure randomly samples inputs of varying lengths (called the "Mix" curriculum in Zaremba & Sutskever (2014)). Additionally, the Control and Program tasks contain complex control flow and nested structure. They are thus a measure of a sequence model's ability to model dependencies of differing lengths, as well as hierarchical information. Thus we are interested in comparing the effects of UGI methods, as well as the full OM- gates which are designed for hierarchical structures (Shen et al., 2018).

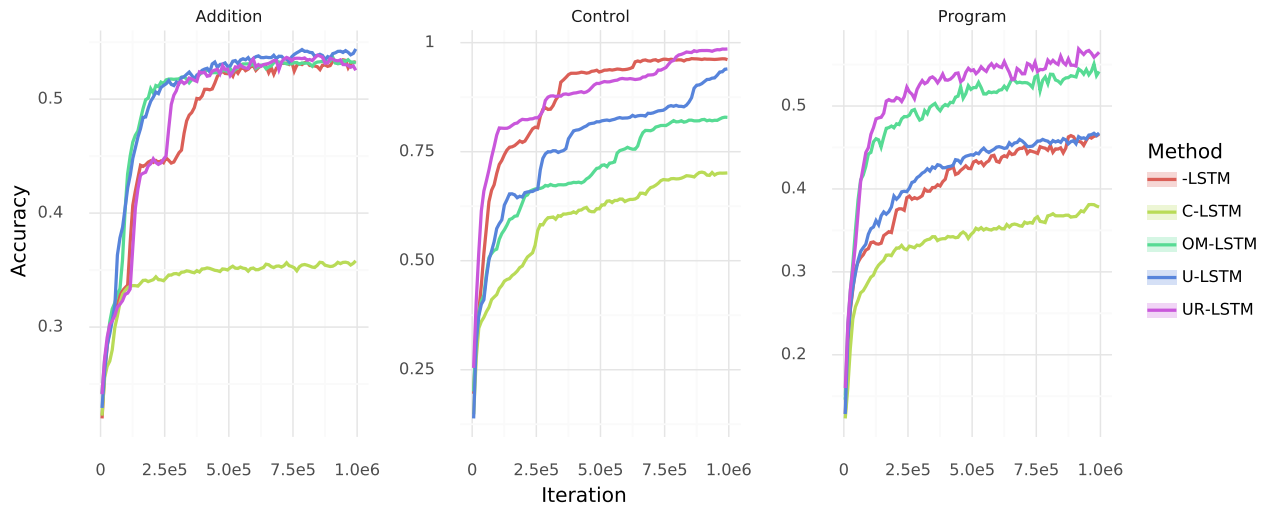
Finally, this task has prior work using a different type of recurrent core, the Relational Memory Core (RMC), that we also use as a baseline to evaluate our gates on different models (Santoro et al., 2018). Both the LSTM and RMC were found to outperform other recurrent baselines such as the Differential Neural Computer (DNC) and EntNet.

Training curves are shown in Figure 14, which plots the median accuracy with confidence intervals. We point out a few observations. First, despite having a T_{max} value on the right order of magnitude, the C- gated methods have very poor performance across the board, reaffirming the chrono initialization's high sensitivity to this hyperparameter.

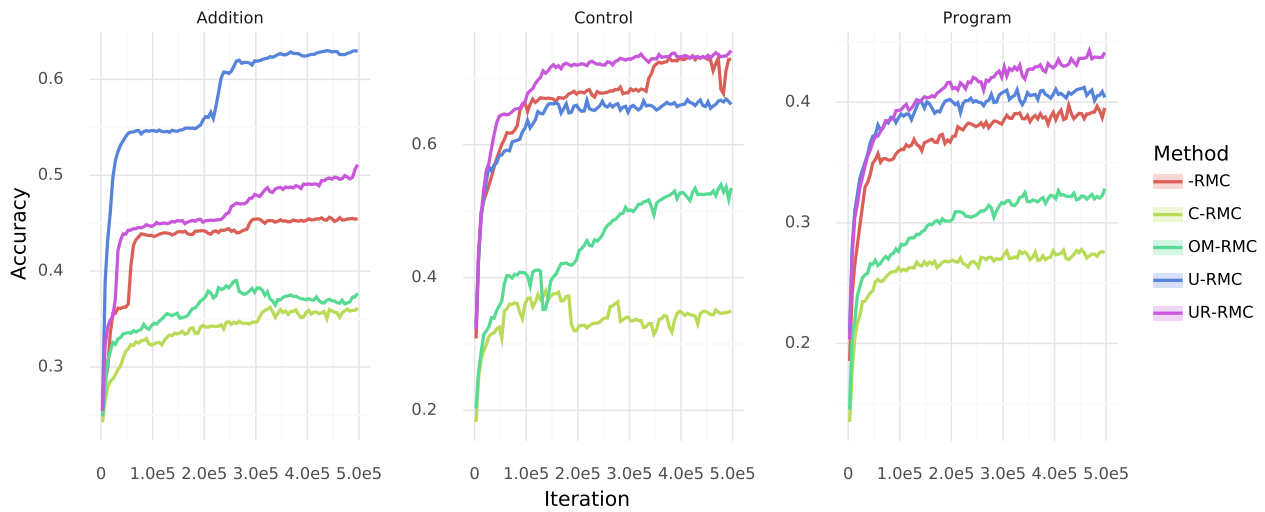
Second, the U-LSTM and U-RMC are the best methods on the Addition task. Additionally, the UR-RMC vs. RMC on Addition is one of the very few tasks we have found where a generic substitution of the UR- gate does not improve on the basic gate. We have not investigated what property of this task caused these phenomena.

Aside from the U-LSTM on addition, the UR-LSTM outperforms all other LSTM cores. The UR-RMC is also the best core on both Control and Program, the tasks involving hierarchical inputs and longer dependencies. For the most part, the improved mechanisms of the UR- gates seem to transfer to this recurrent core as well. We highlight that this is not true of similar gating mechanisms. In particular, the OM-LSTM, which is supposed to model hierarchies, has good performance on Control and Program as expected (although not better than the UR-LSTM). However, the OM- gates' performance plummets when transferred to the RMC core.

Interestingly, the -LSTM cores are consistently better than the -RMC versions, contrary to previous findings on easier versions of this task using similar protocol and hyperparameters (Santoro et al., 2018). We did not explore different hyperparameter regimes on this more difficult setting.



(a) LSTM - Learning to Execute (nesting=4, length=9)



(b) RMC - Learning to Execute (nesting=4, length=9)

Figure 14. Program Execution evaluation accuracies.